

# Geophysical Research Letters<sup>®</sup>



## RESEARCH LETTER

10.1029/2021GL097345

### Key Points:

- Massive turbulence data sets from multiyear time series at sites in Pacific and Atlantic cold tongues are compared
- Diurnal composites document similarities in variability and magnitudes of deep cycle turbulence in Atlantic and Pacific cold tongues
- A depth/amplitude scaling collapses turbulence dissipation measurements at three cold tongue sites to within a factor of 2

### Correspondence to:

J. N. Moum,  
[jim.moum@oregonstate.edu](mailto:jim.moum@oregonstate.edu)

### Citation:

Moum, J. N., Hughes, K. G., Shroyer, E. L., Smyth, W. D., Cherian, D., Warner, S. J., et al. (2022). Deep cycle turbulence in Atlantic and Pacific cold tongues. *Geophysical Research Letters*, 49, e2021GL097345. <https://doi.org/10.1029/2021GL097345>

Received 9 DEC 2021  
Accepted 31 MAR 2022



### Author Contributions:

**Conceptualization:** James N. Moum  
**Data curation:** Marcus Dengler  
**Formal analysis:** James N. Moum  
**Funding acquisition:** James N. Moum  
**Methodology:** James N. Moum, Emily L. Shroyer  
**Software:** Kenneth G. Hughes, Sally J. Warner  
**Writing – original draft:** James N. Moum  
**Writing – review & editing:** Kenneth G. Hughes, Emily L. Shroyer, William D. Smyth, Deepak Cherian, Sally J. Warner, Bernard Boulès, Peter Brandt, Marcus Dengler

© 2022. The Authors.

This is an open access article under the terms of the [Creative Commons Attribution-NonCommercial-NoDerivs License](https://creativecommons.org/licenses/by-nc-nd/4.0/), which permits use and distribution in any medium, provided the original work is properly cited, the use is non-commercial and no modifications or adaptations are made.

## Deep Cycle Turbulence in Atlantic and Pacific Cold Tongues

James N. Moum<sup>1</sup> , Kenneth G. Hughes<sup>1</sup>, Emily L. Shroyer<sup>2</sup>, William D. Smyth<sup>1</sup>, Deepak Cherian<sup>3</sup>, Sally J. Warner<sup>4</sup>, Bernard Boulès<sup>5</sup> , Peter Brandt<sup>6,7</sup> , and Marcus Dengler<sup>6</sup> 

<sup>1</sup>College of Earth, Ocean, and Atmospheric Sciences, Oregon State University, Corvallis, OR, USA, <sup>2</sup>Office of Naval Research, Arlington, VA, USA, <sup>3</sup>National Center for Atmospheric Research, Boulder, CO, USA, <sup>4</sup>Department of Physics and Environmental Studies, Brandeis University, Waltham, MA, USA, <sup>5</sup>Institut de Recherche pour le Développement, Brest, France, <sup>6</sup>GEOMAR Helmholtz Centre for Ocean Research Kiel, Kiel, Germany, <sup>7</sup>Kiel University, Kiel, Germany

**Abstract** Multiyear turbulence measurements from oceanographic moorings in equatorial Atlantic and Pacific cold tongues reveal similarities in deep cycle turbulence (DCT) beneath the mixed layer (ML) and above the Equatorial Undercurrent (EUC) core. Diurnal composites of turbulence kinetic energy dissipation rate,  $\epsilon$ , clearly show the diurnal cycles of turbulence beneath the ML in both cold tongues. Despite differences in surface forcing, EUC strength and core depth DCT occurs, and is consistent in amplitude and timing, at all three sites. Time-mean values of  $\epsilon$  at 30 m depth are nearly identical at all three sites. Variations of averaged values of  $\epsilon$  in the deep cycle layer below 30 m range to a factor of 10 between sites. A proposed scaling in depth that isolates the deep cycle layers and of  $\epsilon$  by the product of wind stress and current shear collapses vertical profiles at all sites to within a factor of 2.

**Plain Language Summary** The equatorial cold tongues are large areas of the ocean that extract a globally disproportionate amount of heat from the atmosphere, and where that heat is mixed downward to the deeper ocean, a critical process in climate regulation. This mixing is dominated by deep cycle turbulence, a well-documented feature of the central equatorial Pacific cold tongue. Poleward of the Equatorial Undercurrent, nighttime cooling of the sea surface causes increases in turbulence to the depth of the mixed layer (ML), typically a few tens of meters, below which turbulence is much reduced. On the equator, in contrast, opposing currents at the surface and roughly 100 m below the surface create a dynamic environment in which nightly increases in turbulence occur over many tens of meters below the ML base. This has been termed DC turbulence. Here, using massive data sets from both Pacific and Atlantic cold tongues, we show that DC turbulence is present at each location and its main characteristics are consistent between them.

## 1. Introduction

Typically, open ocean surface mixed layers away from the equator are driven by a combination of wind stress and convection from nighttime cooling or other forms of cold air outbreaks (Shay & Gregg, 1986) and these mixed layers largely contain the turbulence within (Anis & Moum, 1994). A unique aspect of equatorial small-scale fluid dynamics that has been observed in the Pacific's cold tongue (PCT) at 0°140°W is the existence of diurnally-varying turbulence *beneath* a nighttime surface mixed layer (Lien et al., 1995; Moum et al., 1989). This sub-mixed layer turbulence at the equator has been termed deep cycle (DC) turbulence.

The existence of DC turbulence is linked to the strongly sheared current system above the core of the Equatorial Undercurrent (EUC) where the gradient Richardson number ( $Ri$ ) persistently maintains a near-critical state with values fluctuating around 0.25 (Smyth & Moum, 2013), a state of marginal instability (MI). This persistent MI state is nudged beyond critical toward the end of the solar day, associated with the deepening of the sheared base of the diurnal warm layer that forms during the period of net daytime heating and deepens by shear-induced mixing (K. G. Hughes et al., 2021). A diurnal composite derived from 8 days of microstructure profiling revealed that the shear layer descends from near the surface to about 60 m at a rate close to 6 m per hour (Smyth et al., 2013). The arrival of the shear layer was found to trigger shear instability and also to immediately precede enhanced turbulence, suggesting causality (also, see model results by Pham et al. (2013)).

To summarize, DC turbulence has two defining properties:

1. it occurs below the ML base, and
2. it cycles diurnally.

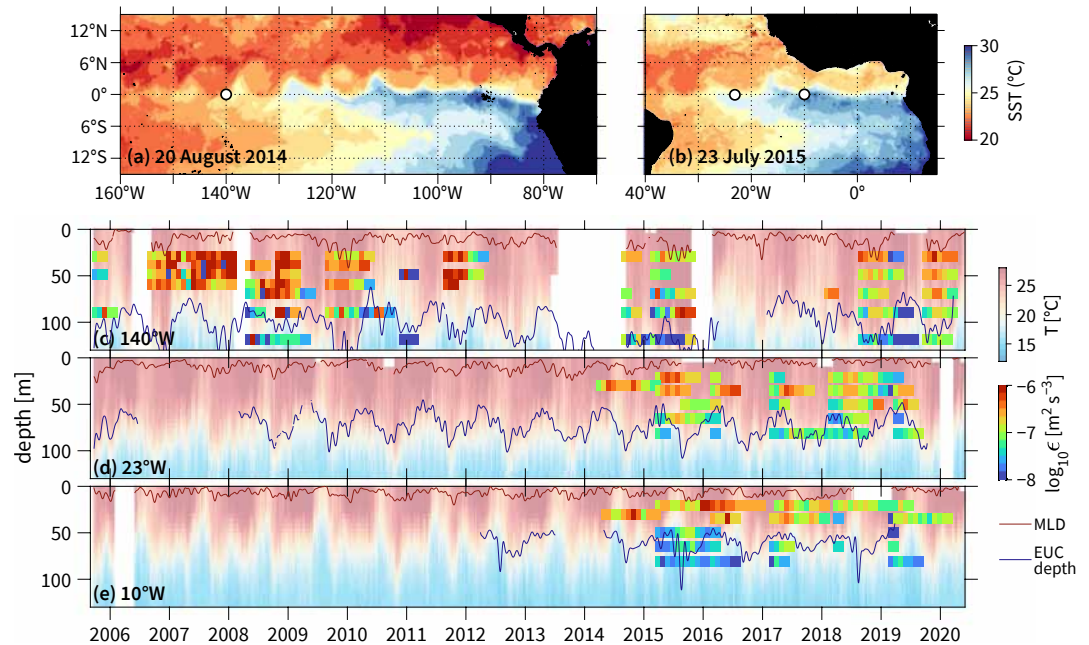


**Figure 1.** Measurements from  $\chi$ pod deployments in the (a) Pacific and (b) Atlantic cold tongues. Time series at (c) 140°W, (d) 23°W and (e) 10°W show colored bars (from monthly averages) to represent turbulence kinetic energy dissipation rate,  $\epsilon$ . Background color is temperature ( $T$ ). Solid white areas indicate lost moorings. Thin red line is the mixed layer (hereafter ML) depth defined as the depth at which  $T$  is smaller by 0.015° from its value at 1 m. Thin blue line is depth of Equatorial Undercurrent (EUC) core, the depth at which the zonal current shear is 0. Nominal  $\chi$ pod depths at 140°W are [30, 50, 70, 90, 120] m with occasional deployments at other depths. Nominal  $\chi$ pod depths at 10°W, 23°W are [20, 35, 50, 65, 80] m.

This contrasts with, for example, turbulence below the ML created by near-inertial wave shear following wind events well away from the equator, as such turbulence does not vary diurnally (Dohan & Davis, 2011; Hummels et al., 2020). Shipboard profiling measurements in the equatorial Pacific (Gregg et al., 1985; Moum & Caldwell, 1985; Moum et al., 1989) reveal both of the defining DC properties, albeit over only the cruise periods (typically a few weeks) and only when profiling was rapid enough to resolve the diurnal cycle. Both shortcomings are addressed using moored measurements.

From hourly-averaged mooring data that did not include turbulence measurements, Pham et al. (2017) showed the existence of the MI state below the ML base, varying diurnally with nighttime minima of  $Ri$ , in all seasons over the 9-year period 1998–2007. In lieu of direct microstructure measurements, they conducted large-eddy simulations, with observationally-based initial and boundary conditions, to confirm that the observed MI state was indicative of turbulence. Daily-averaged mooring data can test for property (1), but not (2). Taking advantage of the greater availability of daily-averaged data, Pham et al. (2017) showed that the MI state existed in the PCT in all seasons over the 20-year period 1990–2010, confirming the persistence of property (1).

In the Atlantic's cold tongue (ACT), Hummels et al. (2013) documented property (1) by combining shipboard data taken at various times and locations. However, Hummels et al. (2013) did not find a clear diurnal cycle (property 2) in the ACT, likely due to limited data availability. Wenegrat and McPhaden (2015) did observe a diurnal in shear and stratification at the equator and 23°W such as to infer DC turbulence but with no turbulence measurements to confirm.

Moored turbulence measurements using  $\chi$ pods (Moum & Nash, 2009) have time resolution sufficient to resolve property (2) and now also extend over many years at a few sites. Data from the  $\chi$ pods at 140°W has shown how the DC varies with the El Niño-Southern Oscillation (ENSO) cycle and is a fundamental part of the underlying Bjerknes feedback (Warner & Moum, 2019) that governs transitions between ENSO phase states.

In the present analysis, we use the several years of moored records of turbulence from  $\chi$ pods at 0°140°W in the PCT (Moum & Nash, 2009), together with two sites in the ACT (Figure 1) to extend our knowledge of the DC by showing that

1. property 2 (diurnal cycling below the ML) exists in both the ACT and the PCT;
2. property 2 is a common feature in diurnally-composited distributions from measurements made over periods of many years;
3. the amplitude and timing of DC turbulence varies with depth and longitude;
4. a scaling of turbulence dissipation by the product of wind stress and current shear, combined with a depth scaling that isolates the DC depth ranges, collapses averaged profiles in ACT and PCT to within a factor of 2.

## 2. Measurements

The measurements discussed here were made from sensors deployed on equatorial moorings at 0°140°W, part of the TAO/TRITON array in the Pacific (McPhaden et al., 1998) and at 0°23°W and 0°10°W, part of the PIRATA array in the Atlantic (Bourlès et al., 2019).

Besides the  $\chi$ pod turbulence measurements, the analysis employs (a) temperature profiles from the main moorings on which the  $\chi$ pods are deployed to determine the time-varying stratification and (b) velocity data from nearby subsurface moorings outfitted with upward-looking acoustic Doppler current profilers (ADCPs). A complete analysis primer (Warner, 2020) describes how the temperature variance dissipation rate ( $\chi$ ), the turbulence kinetic energy dissipation rate ( $\epsilon$ ) and the turbulence diffusivity ( $K_T$ ) are computed from high frequency temperature measurements using fast thermistors on  $\chi$ pods with speed and stratification inputs from the moored temperature and velocity data (Moum & Nash, 2009; Perlin & Moum, 2012; Zhang & Moum, 2010).

We began deploying  $\chi$ pods on the TAO/TRITON mooring at 0°140°W in September 2005 and have attempted to maintain these measurements continually. In 2014, we began deployments of  $\chi$ pods at 0°10°W and 0°23°W. The full records from all  $\chi$ pods at each location are shown in Figure 1.

## 3. Common Features of $\epsilon$ in ACT and PCT

From an 8-day record of shipboard profiling measurements at 0°140°W, Smyth and Moum (2013) showed that there exists a depth range between ML base and EUC core (where zonal current shear vanishes; Figure 2b) over which  $N^2$  and  $Sh^2$  interact in such a manner that  $Ri = N^2/Sh^2$  fluctuates about a critical value,  $Ri_{cr} = 1/4$ . Here,  $N^2 = -g\rho_z/\rho_0$  is the squared buoyancy frequency representing density stratification, where  $\rho$  is the depth-dependent density,  $\rho_0$  is a background reference value, subscript  $z$  represents differentiation with respect to the vertical and  $g$  is Earth's gravitational acceleration. Squared current shear is defined as  $Sh^2 = u_z^2 + v_z^2$ , where  $u$  is the zonal and  $v$  the meridional component of velocity. A useful metric of instability is the percentage of hourly values that are less than  $Ri_{cr}$  (Figure 2c). At and below the mean depths of the EUC core there are very few values of  $Ri < Ri_{cr}$ . This is the case at all three locations (Figure 2c). Upward from the core depths, the frequency of occurrence of  $Ri < Ri_{cr}$  increases, to 75% at 20 m at 140°W and 23°W, and 50% at 10°W. In each case, the 50% metric occurs at roughly 1/2 the distance from the EUC core depth to the sea surface. At 10°W, the depths where  $Ri < Ri_{cr}$  occurs most frequently are likely shallower than 20 m and not sampled by the PIRATA velocity sensors and hence  $Ri$  is not computed there. The ranges of EUC core depths (based on hourly data) are deepest at 140°W and shallow from 23°W to 10°W (Figure 2b).

At the two Atlantic sites, the mean values of  $\epsilon$ , ( $\bar{\epsilon}$ ), are nearly identical at the two uppermost  $\chi$ pods (Figure 2d). At both, the maximum in  $\bar{\epsilon}$  occurs at the second  $\chi$ pod at 30 m. At 140°W the maximum value of  $\bar{\epsilon}$  occurs at 40 m. For each site, the decrease from the respective maxima of  $\bar{\epsilon}$  to its value at EUC core depth is

1. a factor of 10 at 10°W (EUC core at 61 m);
2. a factor of 6 at 23°W (EUC core at 73 m); and
3. a factor of 4 at 140°W (EUC core at 103 m).

Commonalities in the vertical structure and magnitude of the statistic  $\%Ri < 1/4$  are revealed by scaling the depth (where  $z = -\text{depth}$ ) to isolate the DC layer such that the vertical coordinate is  $(z - \text{MLD})/(z_{EUC} - \text{MLD})$ , where MLD is the depth of the ML base and  $z_{EUC}$  is the EUC core depth (Figure 3b). Here and in the subsequent scaling of  $\epsilon$ , daily data are first scaled and then bin-averaged in scaled depth.

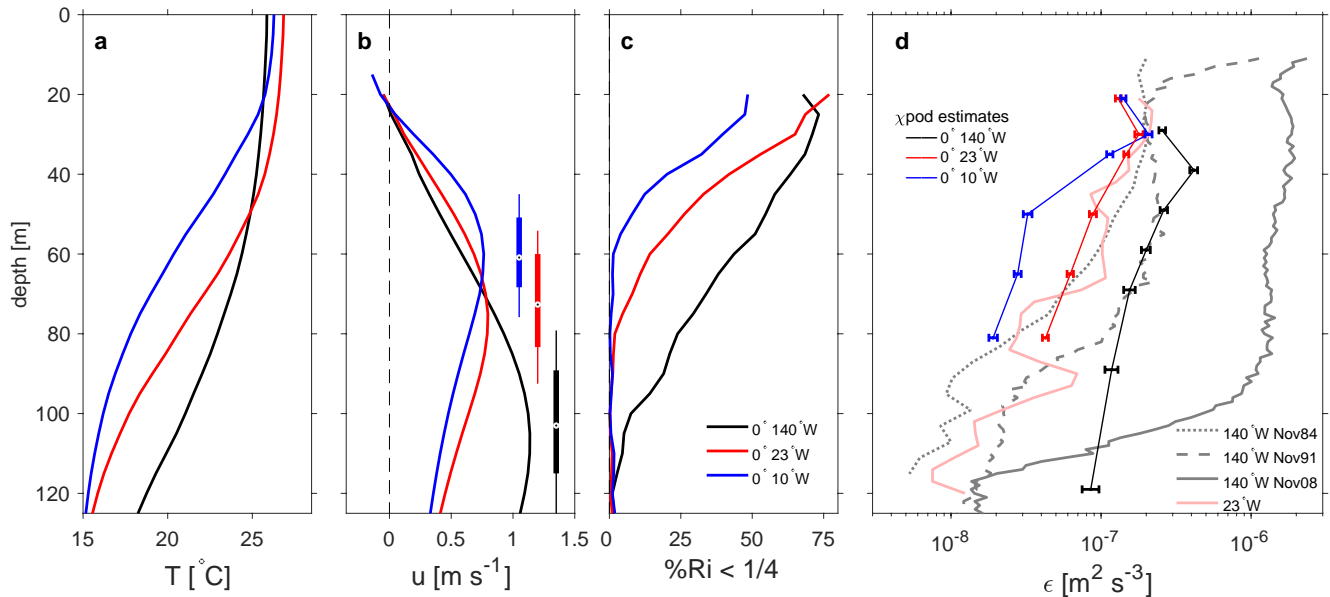


**Figure 2.** Averaged vertical profiles at the equator in the Atlantic’s cold tongue (ACT) (10°W, 23°W; 2013–2019) and Pacific’s cold tongue (PCT) (140°W; 2005–2019). (a) temperature ( $T$ ); (b) zonal velocity ( $u$ ) with the depth of the Equatorial Undercurrent (EUC) core (where  $u_z \rightarrow 0$ ) indicated by vertical bars (25th and 75th percentiles are thick bars and 10th and 90th percentiles are thin bars; statistics from hourly averages). Full current profiles in (b) were constructed with the aid of current meters deployed on the surface mooring to fill in above the upper ADCP range limit at about 40 m depth.; (c) statistic indicating the percentage of time that the gradient Richardson number,  $Ri$ , is less than 1/4 as determined from hourly data; (d) mean values of turbulence dissipation rate,  $\epsilon$ , from  $\chi$ pod estimates with 95% confidence limits computed using non-parametric bootstrap statistics on hourly-averaged data. Averaged vertical profiles are from shipboard experiments at 0°140°W in 1984 (Tropic Heat—1,749 profiles over 12 consecutive days; Moum et al. (1989)), 1991 (Tropical Instability Wave Experiment—3,918 profiles over 22 consecutive days; Lien et al. (1995)) and 2008 (2,624 profiles over 16 consecutive days) (Moum et al., 2009); averages of 154 vertical profiles (red) at 0°23°W taken over 5 mooring deployment cruises during the period 2008–2016, roughly split between boreal spring and boreal autumn (Dengler & Mehrtens, 2021). Note that estimates of  $\epsilon$  for the profiling measurements are derived from shear probe measurements and for the  $\chi$ pod from fast thermistor measurements following Moum and Nash (2009); Zhang and Moum (2010). Hourly temperature data were interpolated to 5 m intervals from nominal sensor depths [0,5,10, 20, 25,40, 45, 60,80, 100, 120,140] m at 140°W and [0,5,10, 20, 40,60, 80, 100,120,140] m at 10°W, 23°W. Moored acoustic Doppler current profilers (ADCP) measurements are provided at 5 m intervals.  $N^2$ ,  $Sh^2$  were then determined by simple differencing over these 5 m intervals.

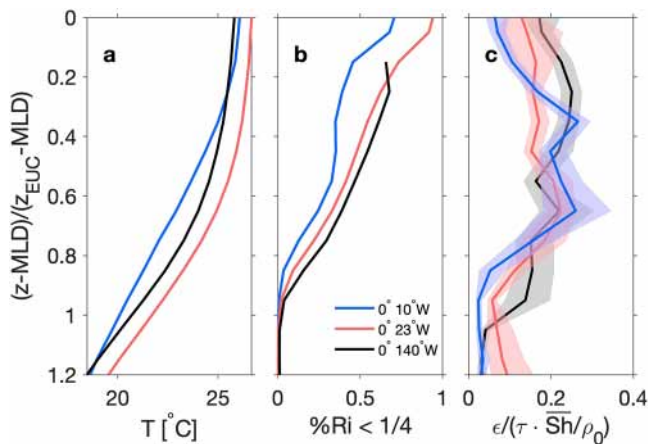


**Figure 3.** Vertical profiles scaled such that the DC layer, from the ML base to the EUC core depth, ranges over 0–1. Scalings employ daily-averaged data.  $z = -\text{depth}$  and  $z > 0$ , upward; MLD is the base of the ML;  $z_{EUC}$  is the EUC core depth. (a)  $T$ ; (b) percentage of values with  $Ri < 1/4$ ; (c)  $\epsilon$  scaled by the product of the wind stress ( $\tau$ ) and  $\overline{Sh}$ , the average value of  $Sh$  over the DC layer, divided by the mean density,  $\rho_0$ . Note the abscissa of (c) is a linear scale. Shading indicates 95% bootstrap confidence limits.

Commonalities in the vertical structure and magnitude of  $\epsilon$  are seen via scaling of  $\epsilon$  by  $\tau \cdot \overline{Sh} / \rho_0$ , where  $\tau$  is the surface wind stress,  $\overline{Sh}$  is the mean value of  $Sh$  over the DC layer and  $\rho_0$  a mean water density (Smyth et al., 2017). This scaling is equivalent to  $u_*^2 \cdot \overline{Sh}$  where the friction velocity  $u_* = \sqrt{\tau / \rho_0}$ . Moum et al. (1989) found the mean value of  $\epsilon / (\tau \cdot \overline{Sh} / \rho_0)$  to be about 0.2 from 12 days of profiling in 1984 at 0°140°W. In Figure 3a, these scalings neatly collapse the vertical profiles of  $\epsilon$  from the three sites to within a factor of 2 at each scaled depth and close to the value of 0.2 found for the limited data set examined by Moum et al. (1989). Note that the model of pulsating DC turbulence derived by Smyth et al. (2017) pertains to night-time only and was tested using data between 20 and 70 m depth in a regime of exceptionally strong DC (November 2008 at 140°W; see (Moum et al., 2009)). In that case the scaled value was 0.86. In contrast, the present test uses long-term averages and therefore includes periods when the DC turbulence is expected to be weak or absent, for example, daytime and spring minima (Pham et al., 2017; Smyth et al., 2021). Using only data from 140°W, (Smyth et al., 2021, their figure B1g) found a scaled dissipation rate of 0.34, consistent (within a factor 2) with Figure 3c. Smyth et al. (2021) also recommended more elaborate scalings designed to capture not only long-term averages but also the more extreme day-to-day fluctuations. Those scalings are not considered here as our interest is the climatology of turbulence in the cold tongues. The latter is best represented by  $\epsilon / (\tau \cdot \overline{Sh} / \rho_0) \approx 0.2$  as is evident in Figure 3c.

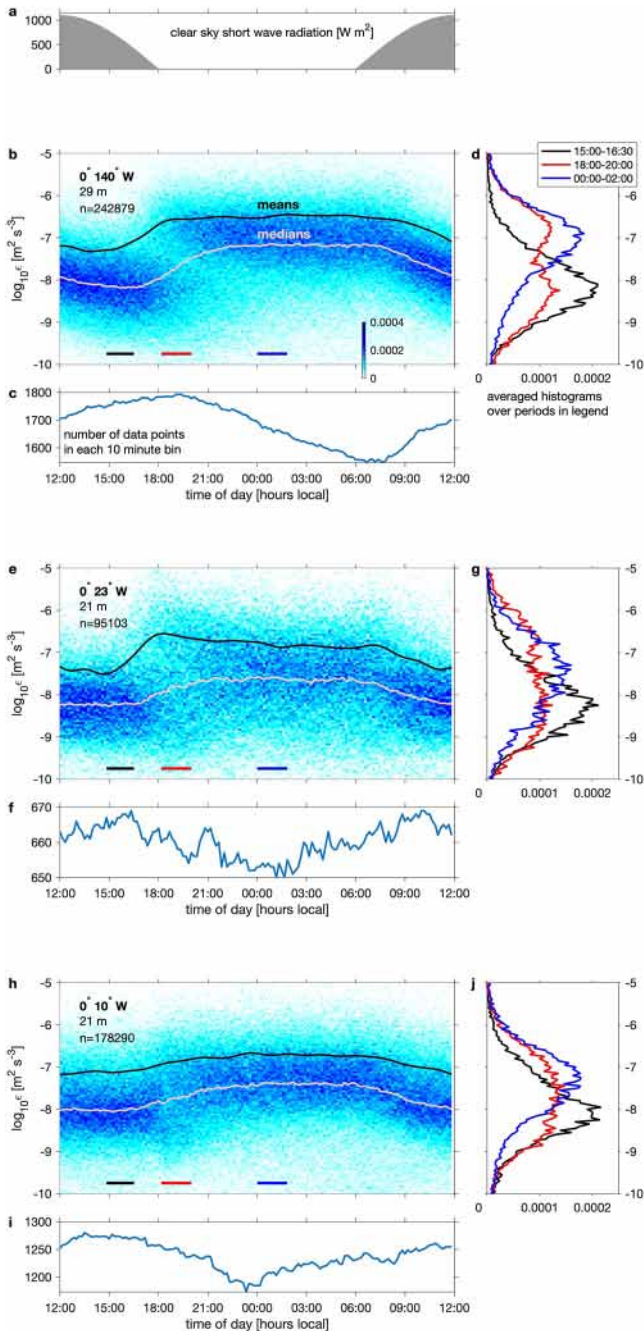


**Figure 4.** (a) Clear sky short wave radiation to solar time (b, e, and h) Diurnally-sorted probability distributions of  $\log_{10} \epsilon$  (increments logarithmically spaced at 0.05) from the uppermost  $\chi$ pod records at the equator and 140°W (b), 23°W (e) and 10°W (h). Black/gray curves represent mean/median values for each 10 min time interval. The value  $n$  at upper left is the number of 10 min intervals represented. (c, f, and i) number of data points in each 10 min time interval. (d, g, and j) One-dimensional histograms of  $\epsilon$  computed by averaging over the time intervals shown in the legend and indicated by the colored bars at the bottom of (b, e, and h).

Figure 2c suggests that  $Ri$  only infrequently decreases below 1/4 at 10°W and this is reflected in the depth-scaled version Figure 2b. The shallower EUC at 10°W means that DC turbulence is confined to a more restricted depth range that is not adequately covered by either our  $\chi$  pods or ADCP measurements. Future PIRATA deployments target this range with  $\chi$  pods and single point velocity measurements above 20 m.

A surprising result from these averaged profiles is that long term mean values of  $\epsilon$  are close to those values from short shipboard experiments executed in the absence of tropical instability waves (TIWs) in 1984 and 1991 (Figure 2d) and an order of magnitude smaller than the 2008 measurements made during the passage of a TIW (shown in Figure 2d as the solid gray line). This suggests that the influence of TIW-induced mixing on long term means is less than expected from the measurements made in 2008 (Inoue et al., 2012, 2019; Moum et al., 2009). The time period of the 2008 experiment is included in the mean  $\chi$ pod estimates of  $\epsilon$  shown in Figure 2d. Confidence in these measurements is justified by previous comparisons between 16-day averages of  $\epsilon$  from (a) shipboard profiling (using shear probes) and (b) multiple  $\chi$  pods on both the TAO mooring and an additional nearby mooring that showed agreement to within a factor of 2 (Perlin & Moum, 2012).

#### 4. Diurnal Variability in ACT and PCT

The existence and behavior of DC turbulence at the equator and 140°W has been well-established through a series of short shipboard profiling investigations there (Gregg et al., 1985; Lien et al., 1995; Moum & Caldwell, 1985; Moum et al., 1989; Smyth et al., 2013). However, details of the averaged vertical structure and indeed the magnitudes of the DC turbulence differed between these necessarily short experiments (Figure 2d). Here we examine diurnal variations in the DC layer using several years of data from  $\chi$  pods at our three locations.

Ensembles of 10-min averaged values of  $\epsilon$ , measured at the uppermost  $\chi$ pod, were binned at 10-min intervals in local time over 24 hr, centered at midnight. Our analysis is intended to reference solar time. On an annual basis, local time differs from solar time by at most 17 min at the equator: sunrise occurs at 06:00 local time  $\pm 17$  min and sunset at 18:00 local time  $\pm 17$  min, the variations being due to the combined effects of Earth's axial tilt and the eccentricity of its orbit, quantified by the equation of time (D. W. Hughes et al., 1989). With 10 min bins, annual variations in solar time relative to local time are less than two bins and use of local time is therefore adequate for the purpose at hand.

Because computation of  $\epsilon$  involves division by  $T_z$  (Moum & Nash, 2009), estimation is avoided for small, uncertain values of  $T_z$  and the data were originally selected by flagging intervals with small values of  $T_z$  ( $< 0.001 \text{ K m}^{-1}$ ) as would occur in the ML. At 29 m depth and 0°140°W the data consists of 242,879 independent 10-min intervals representing 1,686 days (Figure 4b). Due to flagging for small values of  $T_z$ , fewer data points are found at times later in the night when the ML infrequently descends to 29 m at the Pacific location (Figure 4c) and somewhat earlier to 21 m at the Atlantic sites (Figures 4f and 4i). The uppermost  $\chi$  pods at all three locations are significantly deeper than the 90th percentile of ML depths.

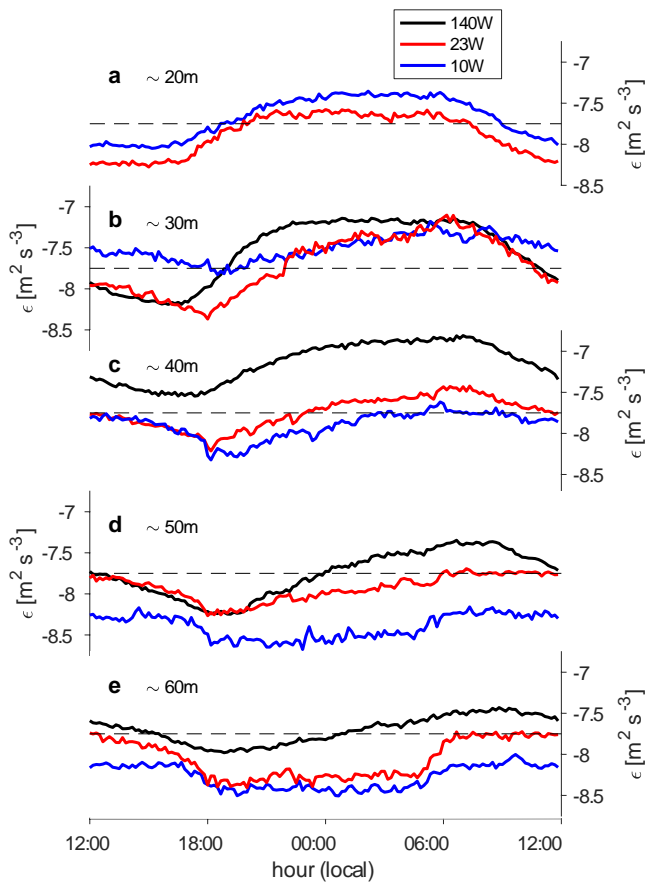


**Figure 5.** Median values of  $\epsilon$  at 20–60 m depth as a function of local time. The two series at 20 m represent the uppermost  $\chi$ pod at 10°W and 23°W and replicate the median lines in Figures 4e and 4h. The black series at 30 m (the uppermost  $\chi$ pod at 140°W) replicates the median line in Figure 4b. The depths shown here are within 5 m of deployed depths.

Systematic diurnal changes are clear in the variability of  $\epsilon$  at 0°140°W as indicated by the progression of the cloud of points representing the time-dependent probability distributions in Figure 4b. There is a general decrease in  $\epsilon$  beginning after sunrise and continuing to sunset. Around sunset, there is an impulse-like increase in  $\epsilon$  from daytime values to a range of values that remains relatively steady until sunrise. Day to night increases of both means and medians are about a factor of 10. Modes differ by more than a factor of 10 (Figure 4d) as indicated by the averaged distributions of  $\epsilon$  before (black—15:00–16:30) and after (blue—00:00–02:00) the sunset transition.

This general pattern of diurnal variation of  $\epsilon$  is repeated at both the 23°W and 10°W sites (Figures 4e–4i). Daytime values are roughly the same as at the 140°W site. Nighttime values are smaller at 10°W and 23°W (Figure 5). At 30 m depth (typically near the uppermost extent of the DC), the sharp day to night transition in mean values of  $\epsilon$  at 23°W is similar to that at 140°W and less so at 10°W. The diurnal variation of the median value of  $\epsilon$  is apparent at all three sites at all depths to 60 m (Figure 5). With increasing depth, the transition to larger nighttime values is delayed in time and reduced in magnitude, which is consistent with DC turbulence being a cycle triggered by surface changes.

The turbulence at 50 m (10°W) and 60 m (10°W, 23°W) is actually reduced at night. At these locations, these depths are strongly stratified and frequently at or below the EUC core depth (Figures 2a and 2b) where we would not expect a connection to DC turbulence. We do not presently have a good idea for the timing of this behavior.

At both PCT and ACT locations, distributions of 10-min averages taken at the uppermost  $\chi$ pod show the dominance of low values in the afternoon, high values after midnight, and a broad, nearly bimodal combination of both during the transition (Figure 4, 18:00–20:00). This apparent bimodal structure is largely associated with an additional dependence on the magnitude of the local wind stress that controls the timing of the transition.

## 5. Conclusions

The 15 years of  $\chi$ pod measurements at 0°140°W provide a different perspective of DC turbulence from the short shipboard experiments previously executed there. Most importantly, they show DC turbulence to be a robust feature that clearly stands out over the multiyear record (Figure 4).

This manuscript describes our first comprehensive look at the  $\chi$ pod records from the ACT. Comparisons to measurements from the PCT at 0°140°W shows the sites at 0°10°W and 0°23°W to exhibit the salient characteristics of the diurnal cycle of turbulence beneath the ML that we associate with DC turbulence. That is, at all three sites, the turbulence extends below the ML base and cycles diurnally (properties 1 and 2 listed in the Introduction). These comparisons also show the averaged magnitudes of  $\epsilon$  near 30 m depth to be consistent within a factor of two at the three sites. While depth dependence varies considerably, the comparisons also support a depth scaling that isolates the relative deep cycle layers with scaling of  $\epsilon$  by  $\tau \cdot \overline{Sh} / \rho_0$ . This combination of depth and amplitude scalings collapses the measurements at the three sites to within a factor of 2 at all depths.

The diurnal composite distributions of Figure 4 indicate that the temporal structure of DC turbulence is present at all of the sites, and the scalings indicate a consistency between them. This should provide some confidence that DC turbulence is a common feature of the cold tongues in general. While features of DC turbulence have been simulated by Pei et al. (2020) in a global ocean general circulation model, quantification of the full zonal and meridional extent of DC turbulence via direct measurement remains an outstanding and important task.

## Data Availability Statement

$\chi$ pod data, ancillary data, mooring details and history are available at NOAA's Global Tropical Moored Buoy Array. TAO and PIRATA data (including  $\chi$ pod data) are directly accessed from <https://www.pmel.noaa.gov/tao/drupal/disdsl/>.

## Acknowledgments

The measurements described here have been fully funded by the National Science Foundation (grants 1256620, 1431518, 2048631). We acknowledge the efforts of past and present Ocean Mixing Group engineers M. Neeley-Brown, R. Kreth, A. Perlin, M. Borgerson, C. Van Appledorn, P. Vutukur, K. Latham and J. Logan in building, testing and calibrating  $\chi$ pods. We are grateful for the assistance of NOAA's National Data Buoy Center who deploy and recover instruments on the TAO/TRITON array and to NOAA's Pacific Marine Environmental Lab who coordinate shipments including our  $\chi$ pods to IRD (France) for deployment and recovery of the instruments on the PIRATA array and to IRD's "IMAGO unit", led by Fabrice Roubaud and Pierre Rousselot, who direct the mooring and  $\chi$ pod deployments for French Pirata cruises. W. D. Smyth and J. N. Moum acknowledge support from the National Science Foundation under Grant 1851520. P. Brandt and M. Dengler acknowledge support from the EU H2020 program (grants 817578 TRIATLAS and 101003470 NextGEMS).

## References

- Anis, A., & Moum, J. N. (1994). Prescriptions for heat flux and entrainment rate in the upper ocean during convection. *Journal of Physical Oceanography*, *24*, 2142–2155. [https://doi.org/10.1175/1520-0485\(1994\)024<2142:pfhfae>2.0.co;2](https://doi.org/10.1175/1520-0485(1994)024<2142:pfhfae>2.0.co;2)
- Bourlès, B., Araujo, M., McPhaden, M. J., Brandt, P., Foltz, G. R., Lumpkin, R., et al. (2019). Pirata: A sustained observing system for Tropical Atlantic climate research and forecasting. *Earth and Space Science*, *6*, 577–616. <https://doi.org/10.1029/2018EA000428>
- Dengler, M., & Mehrtens, H. (2021). *Data from: Sfb754 turbulence measurements (mss)*. WorldData Center. <https://doi.org/10.1594/PANGAEA.926518>
- Dohan, K., & Davis, R. E. (2011). Mixing in the transition layer during two storm events. *Journal of Physical Oceanography*, *41*, 42–66. <https://doi.org/10.1175/2010JPO4253.1>
- Gregg, M. C., Peters, H., Wesson, J. C., Oakey, N. S., & Shay, T. J. (1985). Intensive measurements of turbulence and shear in the Equatorial Undercurrent. *Nature*, *318*, 140–144. <https://doi.org/10.1038/318140a0>
- Hughes, D. W., Yallop, B., & Hohenkerk, C. (1989). The equation of time. *Monthly Notices of the Royal Astronomical Society*, *238*, 1529–1535. <https://doi.org/10.1093/mnras/238.4.1529>
- Hughes, K. G., Moum, J. N., Shroyer, E. L., & Smyth, W. D. (2021). Stratified shear instabilities in diurnal warm layers. *Journal of Physical Oceanography*. <https://doi.org/10.1175/JPO-D-20-0300.1>
- Hummels, R., Dengler, M., & Bourlès, B. (2013). Seasonal and regional variability of upper ocean diapycnal heat flux in the Atlantic cold tongue. *Progress in Oceanography*, *111*, 52–74. <https://doi.org/10.1016/j.pocean.2012.11.001>
- Hummels, R., Dengler, M., Rath, W., Foltz, G., Schütte, F., Fischer, T., & Brandt, P. (2020). Surface cooling caused by rare but intense near-inertial wave induced mixing in the Tropical Atlantic. *Nature Communications*, *43*. <https://doi.org/10.1038/s41467-020-17601-x>
- Inoue, R., Lien, R.-C., & Moum, J. N. (2012). Modulation of equatorial turbulence by a tropical instability wave. *Journal of Geophysical Research*, *117*. <https://doi.org/10.1029/2011JC007767>
- Inoue, R., Lien, R.-C., Moum, J. N., Perez, R. C., & Gregg, M. C. (2019). Variations of equatorial shear, stratification, and turbulence within a tropical instability wave cycle. *Journal of Geophysical Research: Oceans*, *124*(3), 1858–1875. <https://doi.org/10.1029/2018JC014480>
- Lien, R., Caldwell, D. R., Gregg, M. C., & Moum, J. N. (1995). Turbulence variability in the central Pacific at the beginning of the 1991–93 El Niño. *Journal of Geophysical Research*, *100*, 6881–6898. <https://doi.org/10.1029/94JC03312>
- McPhaden, M., Busalacchi, A., Cheney, R., Donguy, J.-R., Gage, K. S., Halpern, D., et al. (1998). The tropical ocean-global atmosphere observing system: A decade of progress. *Journal of Geophysical Research*, *103*, 14169–14240. <https://doi.org/10.1029/97JC02906>
- Moum, J. N., & Caldwell, D. R. (1985). Local influences on shear flow turbulence in the Equatorial Ocean. *Science*, *230*, 215–315. <https://doi.org/10.1126/science.230.4723.315>
- Moum, J. N., Caldwell, D. R., & Paulson, C. A. (1989). Mixing in the equatorial surface layer and thermocline. *Journal of Geophysical Research*, *94*, 2005–2021. <https://doi.org/10.1029/JC094iC02p02005>
- Moum, J. N., Lien, R.-C., Perlin, A., Nash, J. D., Gregg, M. C., & Wiles, P. J. (2009). Sea surface cooling at the equator by subsurface mixing in tropical instability waves. *Nature Geoscience*, *2*, 761–765. <https://doi.org/10.1038/ngeo657>
- Moum, J. N., & Nash, J. D. (2009). Mixing measurements on an Equatorial Ocean mooring. *Journal of Atmospheric and Oceanic Technology*, *26*, 317–336. <https://doi.org/10.1175/2008JTECHO617.1>
- Pei, S., Shinoda, T., Wang, W., & Lien, R.-C. (2020). Simulation of deep cycle turbulence by a global ocean general circulation model. *Geophysical Research Letters*, *47*. <https://doi.org/10.1029/2020GL088384>
- Perlin, A., & Moum, J. N. (2012). Comparison of thermal variance dissipation rates from moored and profiling instruments at the equator. *Journal of Atmospheric and Oceanic Technology*, *29*, 1347–1362. <https://doi.org/10.1175/JTECH-D-12-00019.1>
- Pham, H., Sarkar, S., & Winters, K. B. (2013). Large-eddy simulation of deep-cycle turbulence in an Equatorial Undercurrent model. *Journal of Physical Oceanography*, *43*, 2490–2502. <https://doi.org/10.1175/JPO-D-13-016.1>
- Pham, H., Smyth, W. D., Moum, J. N., & Sarkar, S. (2017). Seasonality of deep cycle turbulence in the eastern equatorial Pacific. *Journal of Physical Oceanography*, *47*, 2189–2209. <https://doi.org/10.1175/JPO-D-17-0008.1>
- Shay, T. J., & Gregg, M. C. (1986). Convectively driven turbulent mixing in the upper ocean. *Journal of Physical Oceanography*, *16*, 1777–1798. [https://doi.org/10.1175/1520-0485\(1986\)016<1777:cdtmit>2.0.co;2](https://doi.org/10.1175/1520-0485(1986)016<1777:cdtmit>2.0.co;2)
- Smyth, W. D., & Moum, J. N. (2013). Marginal instability and deep cycle mixing in the eastern equatorial Pacific Ocean. *Geophysical Research Letters*, *40*, 6181–6185. <https://doi.org/10.1002/2013GL058403>
- Smyth, W. D., Moum, J. N., Li, L., & Thorpe, S. A. (2013). Diurnal shear instability, the descent of the surface shear layer and the deep cycle of equatorial turbulence. *Journal of Physical Oceanography*, *43*, 2432–2455. <https://doi.org/10.1175/JPO-D-13-089.1>
- Smyth, W. D., Pham, H., Moum, J. N., & Sarkar, S. (2017). Pulsating stratified turbulence in the upper Equatorial Oceans. *Journal of Fluid Mechanics*, *822*, 327–341. <https://doi.org/10.1017/jfm.2017.283>
- Smyth, W. D., Warner, S. J., Moum, J. N., Pham, H., & Sarkar, S. (2021). What controls the deep cycle? Proxies for equatorial turbulence. *Journal of Physical Oceanography*, *51*, 2291–2302. <https://doi.org/10.1175/JPO-D-20-0236.1>
- Warner, S. J. (2020).  $\chi$ pod and GusT processing manual. Oregon State University. Retrieved from [https://ir.library.oregonstate.edu/concern/technical\\_reports/r207tw79j](https://ir.library.oregonstate.edu/concern/technical_reports/r207tw79j)
- Warner, S. J., & Moum, J. N. (2019). Feedback of mixing to ENSO phase change. *Geophysical Research Letters*, *46*(23), 13920–13927. <https://doi.org/10.1029/2019gl085415>
- Wenegrat, J., & McPhaden, M. (2015). Dynamics of the surface layer diurnal cycle in the equatorial Atlantic Ocean (0°, 23°W). *Journal of Geophysical Research*, *120*(1), 563–581. <https://doi.org/10.1002/2014JC010504>
- Zhang, Y., & Moum, J. N. (2010). Inertial-convective subrange estimates of thermal variance dissipation rate from moored temperature measurements. *Journal of Atmospheric and Oceanic Technology*, *27*, 1950–1959. <https://doi.org/10.1175/2010jtecho746.1>